heritage

MDPI

Article

Metal Artefacts and Remains of Armour from Kozlov Rob Castle: Metallurgical Analyses as a Tool for Identification and Interpretation of Fragmentary Archaeological Finds

Jakob Kraner [1], Tomaž Lazar [2], Miha Mlinar [3] and Jaka Burja [4,5,*]

[1] Impol Group, Partizanska ulica 38, 2310 Slovenska Bistrica, Slovenia; jakob.kraner@impol.si
[2] National Museum of Slovenia, Prešernova 20, 1000 Ljubljana, Slovenia; tomaz.lazar@nms.si
[3] Tolminski Muzej, Mestni trg 4, 5220 Tolmin, Slovenia; miha.mlinar@tol-muzej.si
[4] Institute of Metals and Technology, Lepi pot 11, 1000 Ljubljana, Slovenia
[5] Faculty of Natural Sciences and Engineering, University of Ljubljana, Aškerčeva cesta 12, 1000 Ljubljana, Slovenia
* Correspondence: jaka.burja@imt.si

Abstract: The castle on Kozlov Rob above Tolmin is one of the most important historical sites in western Slovenia. Over the years, large quantities of finds dating from the late medieval and early modern periods have been recovered from the castle ruins in the process of archaeological investigations and construction works. Many of the recovered iron artefacts are extremely difficult to identify due to their fragmentary state. This paper presents the study of four relatively recently discovered artefacts. The available evidence suggests that at least one of them belongs to a helmet, while another has been identified as the remains of a lock. The artefacts were analysed with X-ray radiography and X-ray diffraction. Additionally, samples were taken for microhardness Vickers measurements and metallographic analysis with a light microscope and a scanning electron microscope. Additional microchemical and structural phase analysis were done with the electron microscope. The aim of archaeometallurgical analyses is to contribute to a more precise interpretation and add a new dimension to our knowledge of the castle site at Kozlov Rob.

Keywords: archaeology; castle; Kozlov Rob; Slovenia; armour; helmet; metallography

Citation: Kraner, J.; Lazar, T.; Mlinar, M.; Burja, J. Metal Artefacts and Remains of Armour from Kozlov Rob Castle: Metallurgical Analyses as a Tool for Identification and Interpretation of Fragmentary Archaeological Finds. *Heritage* **2023**, *6*, 4653–4670. https://doi.org/10.3390/heritage6060247

Received: 14 March 2023
Revised: 1 June 2023
Accepted: 2 June 2023
Published: 6 June 2023

1. Introduction

The fortification on Kozlov Rob above Tolmin, also known as Bockstein (Pockstein) in the primary sources, ranks among the most prominent castles in northwest Slovenia (Figure 1a) and represents one of the most important artistic and architectural monuments in the Tolminsko region. The castle, which already stood at this location in the 12th century, was also the seat of the Tolmin gastalds. Its last major renovation took place after the destructive earthquake in 1511, while the final construction works were carried out in 1608. The last owners of the castle were the Coronini Counts, who abandoned the residence of Kozlov Rob in the mid 17th century. By then, the castle was already in a state of disrepair, falling into ruin in the 18th century [1–5].

The first archaeological investigations of the castle site date to the 1960s when the Nova Gorica Institute for the Protection of Monuments cleared the ruins of vegetation to allow measurement and detailed documentation of the castle compound and the exterior walls. Furthermore, two water cisterns in the castle courtyard were archaeologically excavated in 1964 and 1965. The cisterns contained a large quantity of rich pottery finds (fine glazed earthenware tableware, rough kitchenware, stove tiles), glassware, and fragments of minor everyday utensils (such as crockery) as well as weapons (arrowheads, crossbow bolts, and cannonballs) [6–8]. Perhaps the most intriguing among the recovered metal artefacts were two perforated steel plates, whose purpose seemed unclear at first. Extensive research

carried out in recent years revealed that one of them was a recycled fragment of a 15th or 16th century breastplate reused as a grate or vent [9,10].

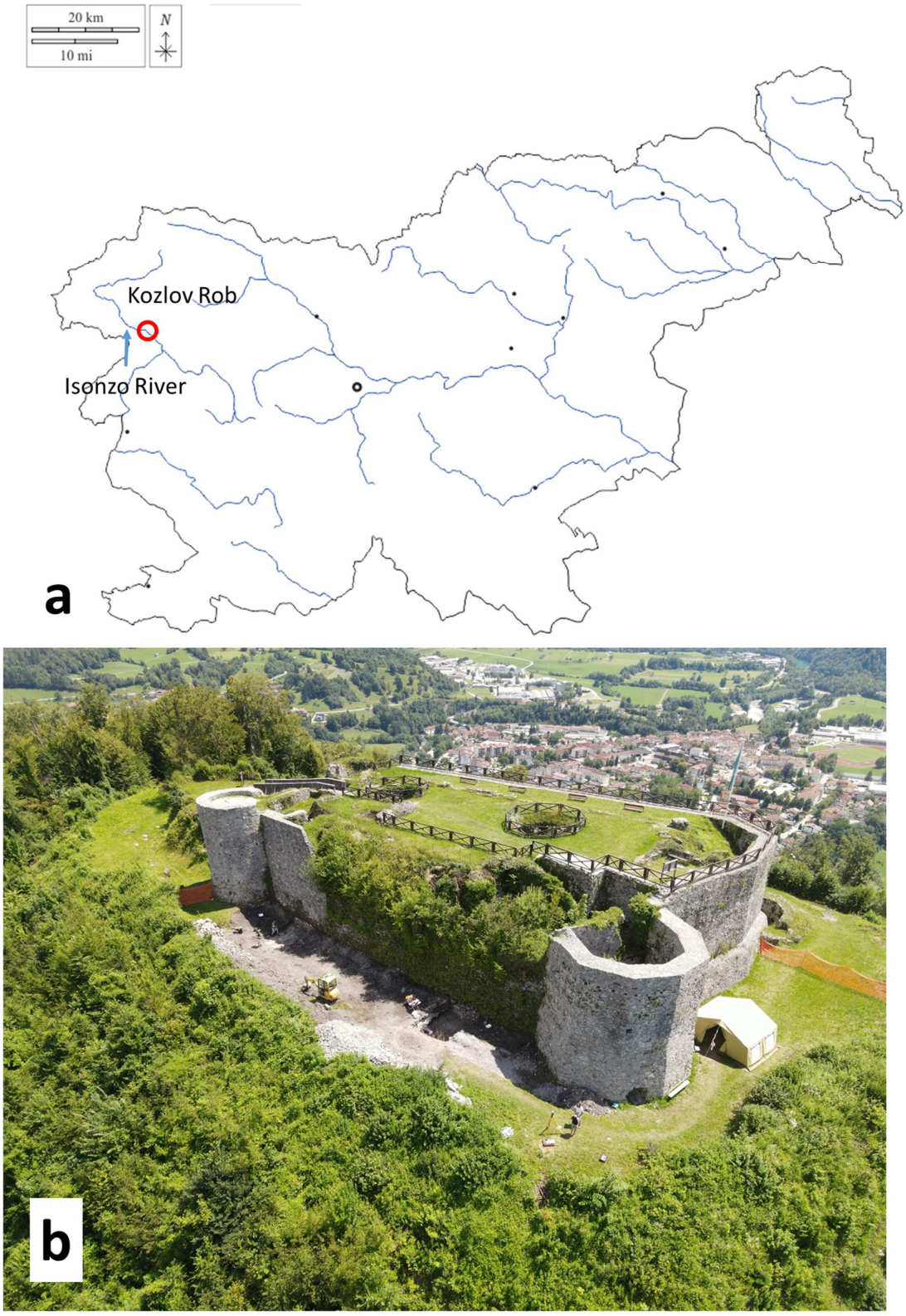

Figure 1. Kozlov Rob castle: (**a**)—its geographic position in Slovenia (red); (**b**)—view of the castle, with Tolmin in the background (Photo archive of the Tolmin Museum).

Between 1996 and 1997, further archaeological investigations were organised by the Department of Archaeology from Ljubljana in collaboration with the Regional Museum Goriški, focusing mostly on the castle courtyard [11].

At the turn of the millennium, the demanding restoration and partial reconstruction of the castle walls began but were never fully completed [12]. The most recent archaeological excavations took place in August 2020 in the north zwinger, or outer courtyard, before the planned restoration and partial reconstruction of the north castle wall. Numerous archaeological finds were discovered in the late medieval and early modern strata dating from the final period of the castle settlement. These include pottery fragments, minor everyday utensils (such as knives, scissors, keys, locks, bronze and silver coins, as well as a Venetian gold coin, a golden and a silver ring), a large quantity of animal bones, and various weapons (crossbow bolts, iron cannonballs) [13,14].

At the very spot of the archaeological excavations from 2020, in the area of the north outer courtyard, specifically on the western side of the northeast tower, construction workers involved in the restoration of the tower and section of the north wall uncovered several finds in September 2003 (Figure 1b): 10 iron cannonballs with diameters ranging from 4.7 to 6.4 cm (kept by the Tolmin Museum, Inv. Nos. TM 729–738), and the initially unidentified iron fragments discussed in this paper. The interpretation of these finds presented a serious problem due to their incomplete shape and advanced state of degradation, made even more challenging by the lack of an easily recognisable archaeological context in mixed landfill deposits where no clear stratigraphic layers could be determined as means of dating the individual items. Their exact nature could only be determined upon completion of archaeometallurgical analyses, which greatly added to the interpretative value of seemingly shapeless archaeological remains and opened up further insights into the history of the Kozlov Rob site. The article presents a detailed account of the results obtained from a variety of light microscopy (LM), scanning electron microscopy (SEM) with energy-dispersive spectroscopy (EDS) or electron back-scatter diffraction (EBSD), and X-Ray analyses on four iron objects excavated from the Kozlov Rob castle.

The use of metallographic analyses in the study of archaeological finds is already well-established [15–17] and has been applied with particular success in the research of historical arms and armour [18–25]. A detailed investigation of historical artefacts, including the materials used for their manufacture, their overall quality, and possible defects, allows for a meaningful explanation of smelting and metalworking techniques employed in the past [19]. The appearance of non-metallic inclusions may often help to differentiate between authentic medieval (or preindustrial) steels and those of a later date [26–30]. However, determining the actual origin of steel artefacts is far more difficult [29,30] and would need to take into account much broader aspects of mineralogy, smelting production, slag analysis [31,32], metal-forming processes [33], as well as heat treatment. Such studies have already been implemented on ancient steel from Egypt, revealing microstructures very similar to those observed in the course of our study [34].

A similar distribution of non-metallic inclusions, according to the flow of deformed material, as well as the presence of the decarburised parts in microstructure, may be observed in artefacts as diverse sources such as finds from China [35] or early modern plate armour of European provenance [19,36]. A number of steel artefacts produced in India, particularly those made from steel sheets, display similar hardness values [37]. The technological similarity between artefacts of such diverse ages and geographic origins suggests that they were produced in a very similar manner, which in itself demonstrates the restrictions of basic metallurgical analyses in dating and identifying historical artefacts. Undoubtedly, a similar approach focusing on the technological make-up of iron or steel artefacts could be applied with success to various other fragmented excavated finds that have proven difficult to identify using more traditional tools of archaeology and historiography.

Further aims of our research were to enhance our understanding of historical metalworking techniques, specifically the production of medieval and early modern steel. Relevant insight into the methods and materials used by historical metallurgists have

been gained by analysing the microstructures and chemical compositions of archaeological iron objects.

2. Materials and Methods

Among the considerable quantity of finds excavated at Kozlov Rob, four rather non-descript artefacts that eluded proper identification by archaeologists and museum curators were selected for detailed analysis. These artefacts are designated as a, b, c, and d, as marked in Figure 2.

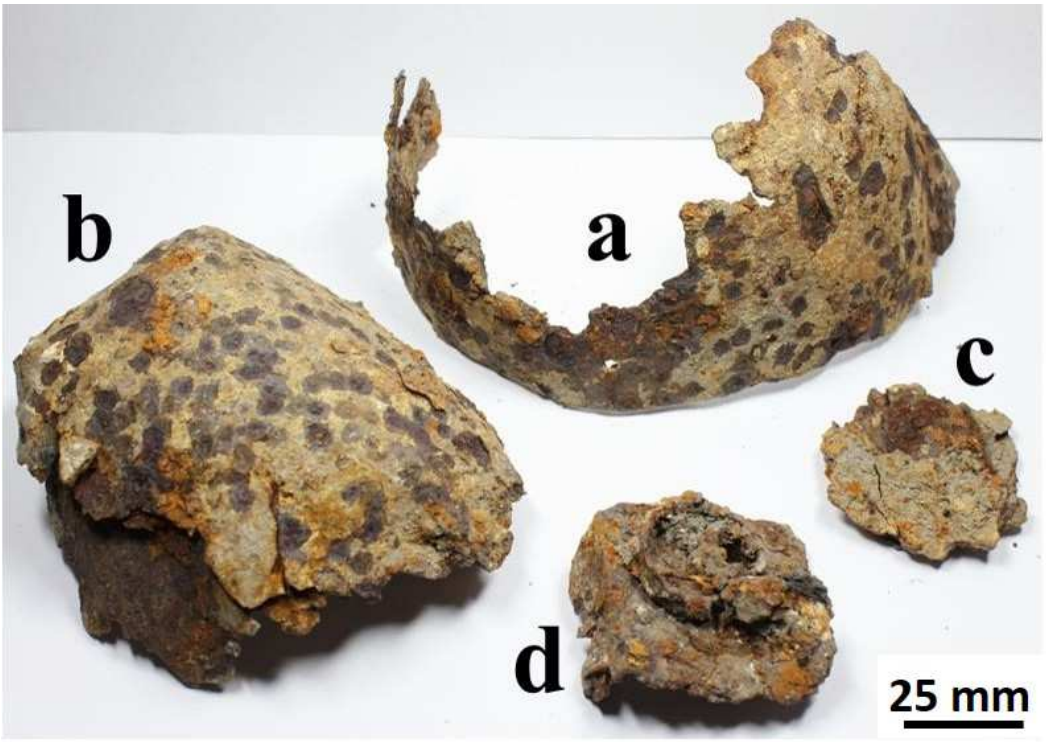

Figure 2. The four investigated artefacts from Kozlov Rob with their corresponding designations: (**a**)—circular shape artefacts, initially suspected fragments of a helmet; (**b**)—circular shape artefacts, also initially suspected fragments of a helmet; (**c**)—a small fragment that can belong to one of the other items; (**d**)—portion of an iron lock.

Each of the four artefacts is discussed separately and individually. Their dimensions are shown in Figure 3. Artefact a is circular, measuring 305 mm along the perimeter. The maximum width of artefact a is 67 mm, and the overall weight is 215.21 g. Five small, circular holes are visible on the bottom, wider section, with each hole measuring around 3 mm in diameter. The distance between them is exactly 41 mm, indicating that they were deliberately punched or drilled. Artefact b is the heaviest in the group, weighing 262.84 g. It has a length of 134 mm and a width of 75 mm. Artefact c is the smallest, weighing only 36.58 g. It measures 59 mm in length and 55 mm in width. Although similar in size, with a length of 57 mm and a width of 54 mm, artefact d is much heavier than artefact c, weighing 63.45 g. The thickness measurements were carried out using a digital micrometre caliper with an accuracy of 0.05 mm.

Three small samples were taken from each of the analysed artefacts following the ASTM E3-11 standard. All 12 sample locations are presented in Figure 3. The dimensions of the samples ranged from 6.0 × 2.4 mm to 14.6 × 9.5 mm (Table 1). The smallest sample (Figure 4a) and the biggest sample (Figure 4b) are shown in Figure 4, captured with the Tegarno FHD digital microscope. The surface of the samples was investigated using the X-ray diffraction (XRD) analysis with the PANalytical 3040 instrument. The samples were cold-mounted in a mixture of 25 g of EpoFix hardener and 3 g of EpoFix

resin for light microscopy (LM) and scanning electron microscopy (SEM). All samples were metallographically prepared (ground and polished) so that their internal structure could be observed using the LM Nikon Microphot FXA microscope. The samples were etched with nital (2.5% HNO_3 and C_2H_5OH). The volume fraction of ferrite (α-Fe, body-centred cubic crystal lattice) and pearlite (eutectoid, αFe + Fe_3C) was determined in accordance with the ASTM E562-19 standard. Furthermore, the C content in steels was determined from the share of phases (Fe-Fe_3C phase diagram) [38].

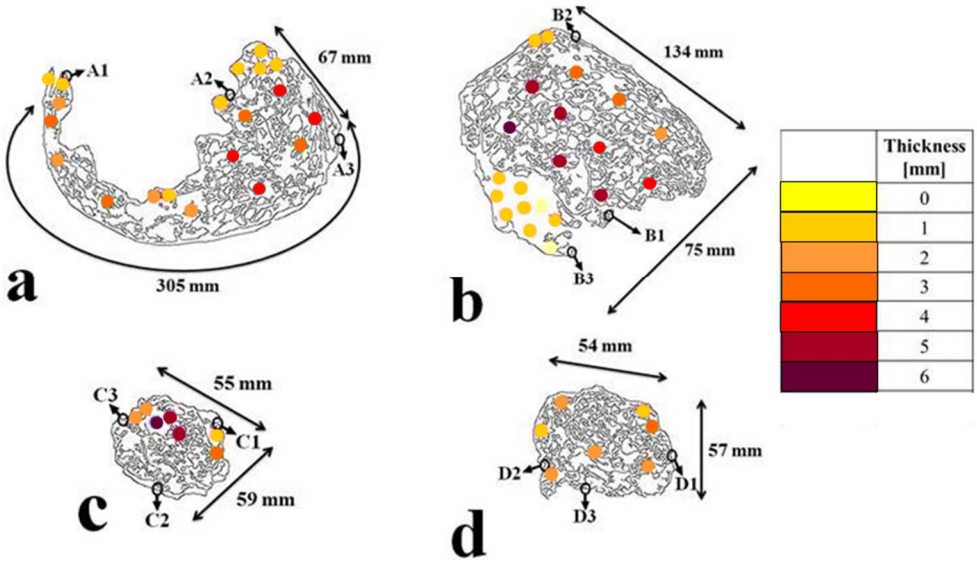

Figure 3. Schematic drawing of the investigated artefacts showing their size and thickness of steel sheet. Three samples were removed from each artefact. Their location is marked with a black circle. (**a**)—circular shape artefact a, suspected helmet; (**b**)—circular shape artefacts b, suspected helmet; (**c**)—a small fragment artefact c; (**d**)—artefact d, portion of an iron lock.

Table 1. List of samples removed from each artefact and their dimensions. The approximate C content was determined on all samples where the metal was sufficiently well-preserved in accordance with the ASTM E562-19 standard.

Artefact	Sample Designation	Dimensions (Length × Height) (mm)	Composition	Approximate C Content (wt.%)
a	A1	8.5 × 2.6	Metal + Scale	0.30 ± 0.05
	A2	7.7 × 5.5	Metal + Scale	0.65 ± 0.08
	A3	18.6 × 7.0	Metal + Scale	0.65 ± 0.10
b	B1	7.5 × 3.9	Scale	/
	B2	6.7 × 1.8	Metal + Scale	0.65 ± 0.10
	B3	9.0 × 6.0	Metal + Scale	0.65 ± 0.10
c	C1	8.1 × 6.8	Scale	/
	C2	8.8 × 8.6	Metal + Scale	0.65 ± 0.11
	C3	14.6 × 9.5	Metal + Scale	0.65 ± 0.08
d	D1	9.3 × 5.1	Scale	/
	D2	8.1 × 4.9	Metal + Scale	0.30 ± 0.04
	D3	6.0 × 2.4	Metal + Scale	0.30 ± 0.05

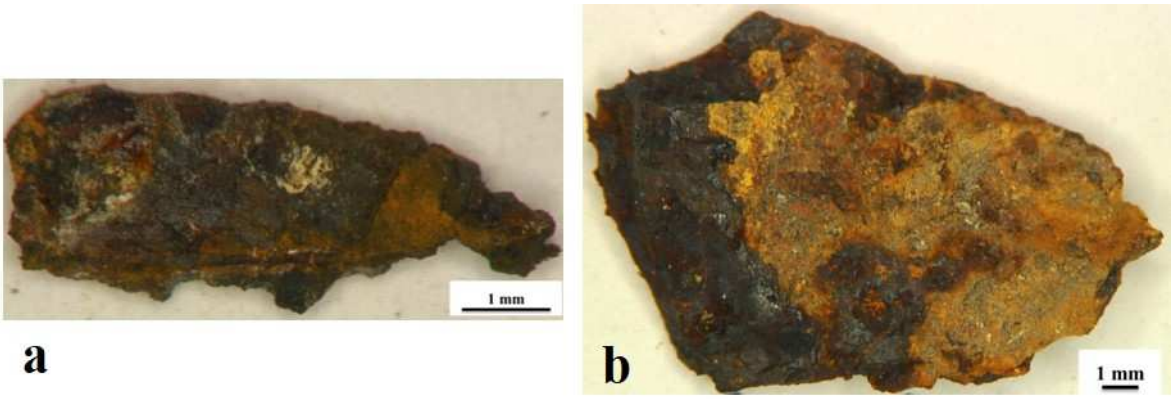

Figure 4. Macrograph of two samples: (**a**)—smallest piece taken from artefact d (D3); (**b**)—largest piece taken from artefact c (C3).

The SEM investigations were carried out with the ZEISS FIBSEM CrossBeam 550. Copper tape was used to ensure the conductivity of the samples. Energy-dispersive X-ray spectroscopy (EDS) was used to determine the chemical composition of the matrix and non-metallic inclusions. For the EDS analysis, the operating voltage of the microscope was set to 15 kV. The crystal grain orientation was observed using electron backscatter diffraction (EBSD) to study the deformation processes and possible heat treatment. The sample was tilted at a 70° angle for the EBSD analysis. During the EBSD investigation, the microscope was set to 19 kV. Hardness was measured using the Vickers method (HV 0.1). Five measurements were taken on each sample, and the hardness results were presented as an average with the deviation. Finally, the artefacts were examined with X-ray radiography in preparation for further conservation treatment. The X-ray radiography was carried out at the Institute of Metal Structures (IMK) in Ljubljana. This technique involves passing X-rays through the object and capturing the resulting shadow image on a detector. Different materials and features within the object absorb X-rays to varying degrees, creating variations in the image density. This technique allows for the visualization of internal details, such as hidden components and structural features.

3. Results

3.1. Thickness Measurements

The thickness of each artefact was measured in various spots, taking into account whether the sheet in that particular location was uniform in cross-section or composed of multiple delaminated layers. Twenty measurements were carried out on artefact a. Its thickness varied between 1.2 mm and 2.5 mm in sections made of a single sheet and from 2.7 mm to 4.5 mm when consisting of multiple layers. On artefact b, the thickness of the sheet was measured at 21 locations. Values ranging from 0.4 mm to 1.9 mm were observed in the case of the single-layer sheet, and between 2.2 mm and 6.8 mm in the case of multiple layers. Seven measurements were carried out on both artefact c and d. The single-layer sheet thickness of artefact c was between 1.9 mm and 3.2 mm. Similar values, from 1.7 mm to 3.5 mm, were observed in the case of artefact d. Some parts of artefact c were composed of multiple layers with a very minor deviation, measuring overall from 5.2 mm to 6.0 mm. No delaminations or multiple layers were observed on artefact d. The measured sheet thicknesses are presented in Figure 3.

3.2. X-ray Diffraction

XRD spectra of the four researched artefacts are presented in Figure 5. The body-centred cubic (BCC) peaks were observed in all four spectra. The first spectrum (artefact a) shows prominent peaks of magnetite and hematite. The spectra of artefacts b and c are very similar. Additionally, a wüstite peak is observed in the case of artefact b, and a cohenite

peak in the spectra of artefact c. BCC and hematite were also found in the fourth spectrum (artefact d), which, in comparison to the other three, shows very weak intensity peaks.

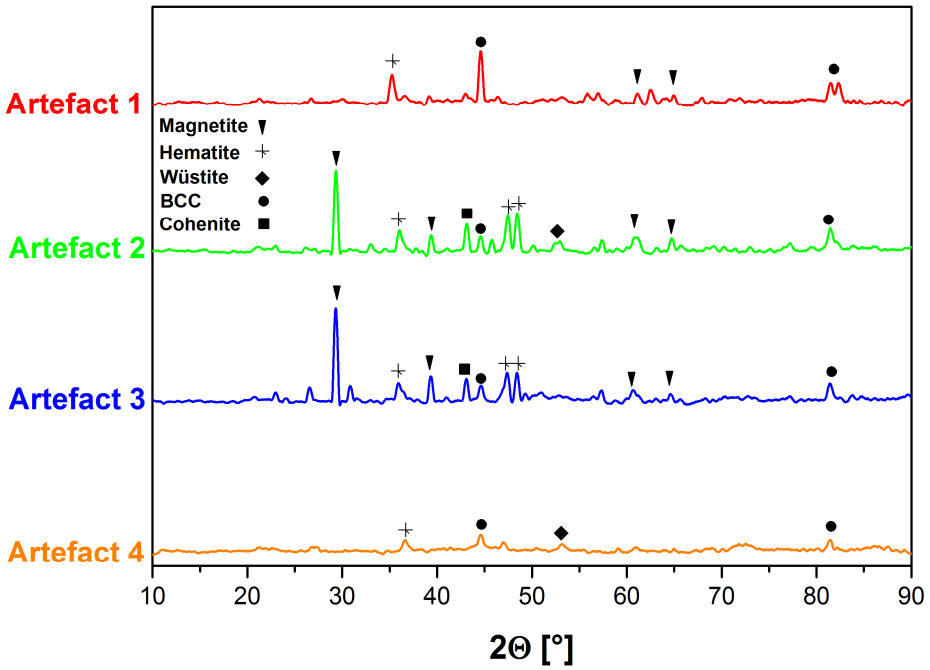

Figure 5. XRD spectra for all four investigated artefacts (samples A2, B2, C2 and D2) in the range of 10 to 90° for 2Θ value, magnetite COD 96-101-1033, hematite COD 96-900-0140, wüstite COD 96-101-1167, BCC COD 96-230-0203, cohenite COD 96-101-0932.

3.3. Light Microscopy

All 12 samples (three from each artefact) were metallographically analysed. Three of them contained only oxide scale, while the remaining nine samples were composed of both metal and scale, so that the C content could be determined. The C content was estimated from the microstructural constituents. As shown in Table 1, the approximate C content is 0.30 wt.% (±0.05) in three samples and 0.65 wt.% (±0.11) in six samples. While artefacts b, c, and d are all made of similar material, the samples taken from artefact a include both lower and higher C content.

The microstructure of the polished sample C3 (artefact c) is presented in Figure 6a. The parallel orientation of the non-metallic inclusions present in the sheet is clearly visible and is evidently the result of the metal-forming technique. Such a flow of non-metallic inclusions is generally associated with the thinning of the material. Some non-metallic inclusions have square shapes, which are typical for undeformable oxides such as aluminium oxides. Samples A1 and A2 were taken from different parts of artefact a, and their microstructures differ greatly. Sample A1 (Figure 6b) consists of acicular ferrite and spheroidised pearlite. Normally, this type of pearlite is formed during annealing after the initial deformation of the material. Based on the microstructure, the C content is estimated to be around 0.30 wt.%. A higher proportion of C, around 0.65 wt.%, and consequently a microstructure with more pearlite, was observed in sample A2 (Figure 6c). The influence of metal forming is still present, as the microstructure is fine-grained. The metallographic analysis reveals the presence of allotriomorphic ferrite (shape of ferrite that follows the grain boundary of prior austenite) around the pearlite grains, indicating air cooling after hot forging. Additionally, some grains are recrystallised. The microstructure of sample B3 (Figure 6d) from artefact b is similar to sample A2, but with visible decarburisation. It demonstrates how deep scale can grow in the metal, so that the area with less C is almost separated from the rest of the material with a higher C content. Figure 6e shows a ferritic-pearlitic microstructure of sample C2 (artefact c). This is quite similar to the microstructures of

samples A2 and B3, with the parallel orientation of non-metallic inclusions being clearly visible. The microstructure also contains cohenite (called cementite needles—Fe_3C in metallography). Ferrite is present along the prior austenite grain boundaries (the specific shape is called allotriomorphic in metallography, and is typical for forged steel). The microstructure in Figure 6f belongs to sample D3 (taken from artefact d), which is quite similar to the microstructure of sample A1. The main differences are the smaller size and slightly tilted orientation of non-metallic inclusions. Carbides are also present, trapped in the corroded layer.

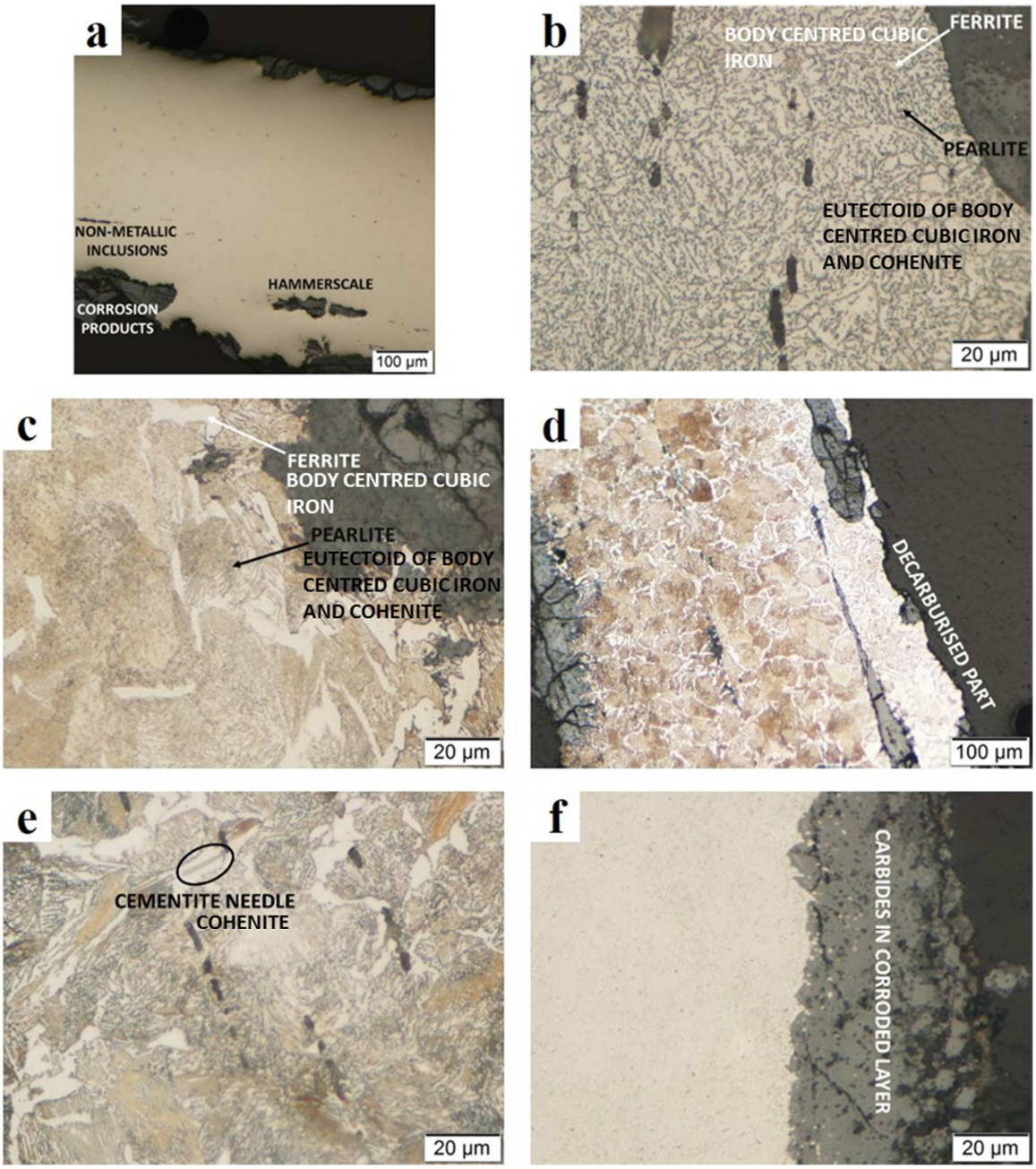

Figure 6. Micrographs made by LM: (**a**)—sample C3 (artefact c) in polished condition; (**b**)—sample A1 (artefact a) with 0.30 wt.% of C content; (**c**)—sample A2 (artefact a) with 0.65 wt.% of C content; (**d**)—sample B3 (artefact b) with decarburisation effect; (**e**)—sample C2 (artefact c) with body centred cubic iron and eutectoid of body centred cubic iron and cohenite (metallographically characterized as allotriomorphic ferrite and pearlite microstructure) and cohenite (cementite needle); (**f**)—sample D3 (artefact d) containing cohenite (carbides) trapped in the oxide layer.

3.4. Scanning Electron Microscopy

EDS spot and area techniques were used to determine the chemical composition of the matrix, scale, and separate (different grayscale) perceived non-metallic inclusions. The selected area one, sample A2, consists only of Fe and O (Figure 7). The proportion between them is 70% and 30%, respectively (Table 2), which is closest to the FeO composition. Selected area two in Figure 7 (sample A2, artefact a) shows the EDS analysis of the matrix. Beside the 94.2 wt.% of Fe, some C was detected, but its content cannot be precisely measured by the EDS method and was therefore omitted from Table 2. The analyses of non-metallic inclusions (spot one, spot three, spot four, and spot five) produced similar results. The alternating dominant contents of Fe, O, and Si range between 19.8 wt.% and 37.2 wt.%. Additionally, Al, Mn, and Ca were detected in the chemical composition of all the investigated spots, though in lower percentages. An exception to these results was observed in the non-metallic inclusion in spot two. Its composition is quite similar to the selected area two, but the proportion between Fe and O (94 wt.% and 5 wt.%) is different due to the small size of the inclusion; a lot of the signal comes from the matrix. SEM-EDS analyses were carried out on all the metallographically prepared samples. The chemical composition of non-metallic inclusions and scale was similar in all cases. Sample A2 was chosen as the most representative, containing different types of non-metallic inclusions.

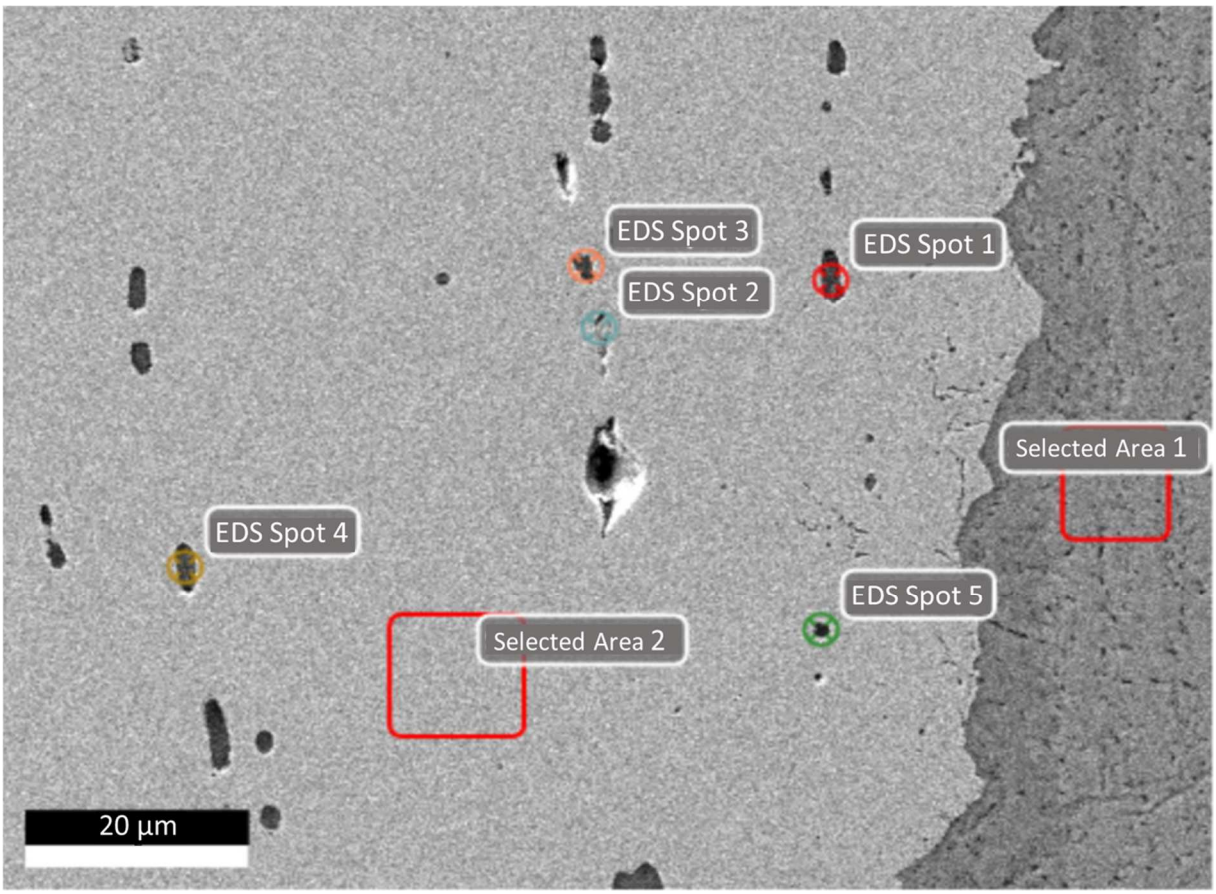

Figure 7. SEM—SEI micrograph of sample A2 with EDS selected spots and areas of analysed matrix, scale, and non-metallic inclusions.

Table 2. Chemical composition (wt.%) of matrix, scale, and non-metallic inclusions determined with spot and area EDS techniques applied on sample A2.

	Fe	O	Si	Al	Mn	Ca
Spot 1 Non-metallic inclusion	31.4	32.3	22.8	4.1	2.8	2.7
Spot 2 Non-metallic inclusion	94.1	5.9	/	/	/	/
Spot 3 Non-metallic inclusion	21.8	37.2	27.3	4.5	3.7	3.8
Spot 4 Non-metallic inclusion	19.8	38.5	28.0	4.2	4.9	2.8
Spot 5 Non-metallic inclusion	35.5	29.4	20.9	2.8	7.2	4.2
Area 1 Scale	70.4	29.6	/	/	/	/
Area 2 Matrix	94.2	/	/	/	/	/

The EDS mapping technique was used to analyse and examine in detail several different non-metallic inclusions. The distribution of elements inside each individual inclusion was further examined in electron back-scattered (BSE) images. Figure 8a (sample C3) shows a typical non-metallic inclusion with a high Si content. The silicon oxides may be present in the ore or even added as a flux; however, auxiliary materials such as clay that contain sand (SiO_2) were also often used to reinforce the walls of medieval smelting furnaces. SiO_2 was introduced in the course of the metallurgical process and is a constant presence in the bloomery process. The flow of material and non-metallic inclusions distributed in the material after forming and deformation are once again clearly shown in Figure 8b (sample B3). The different content of Si in non-metallic inclusions is noticeable, as well as the presence of Al, Mn, and Ca. The difference between non-metallic inclusion and hammerscale is clearly shown in Figure 8c (sample A3). Scale is visible on the right side; it consists solely of Fe and O. Hammerscale typically consists of wüstite (FeO), while other oxides such as hematite (Fe_2O_3) and magnetite (Fe_3O_4) are more often the products of corrosion [39]. Non-metallic inclusions are visible on the left side of Figure 8c (sample A3) Fe and O, Si and other elements are also present, indicating a clear difference from hammerscale.

Additional EBSD investigations revealed further insight into the metal-forming processes. The crystallography of the analysed areas of the artefacts is shown as an inverse pole figure (IPF) in the Z-direction. The crystal grains are coloured in accordance with the key, representing three opposite crystallographic planes {100}, {110}, and {111}. The variety of grain orientation presented in Figure 9 is typical for hand forging and annealing. The grain orientation is defined by the random yet precise operation of the hammer. In our case, the heterogeneous texture of the material is predominant, but the flow of material produced during the thinning of the steel sheet is also clearly visible, especially in the areas of lower deformation (larger grains). Most of the detected grains are smaller than 10 μm. Scale is trapped between the steel matrix on the left and right sides in Figure 9.

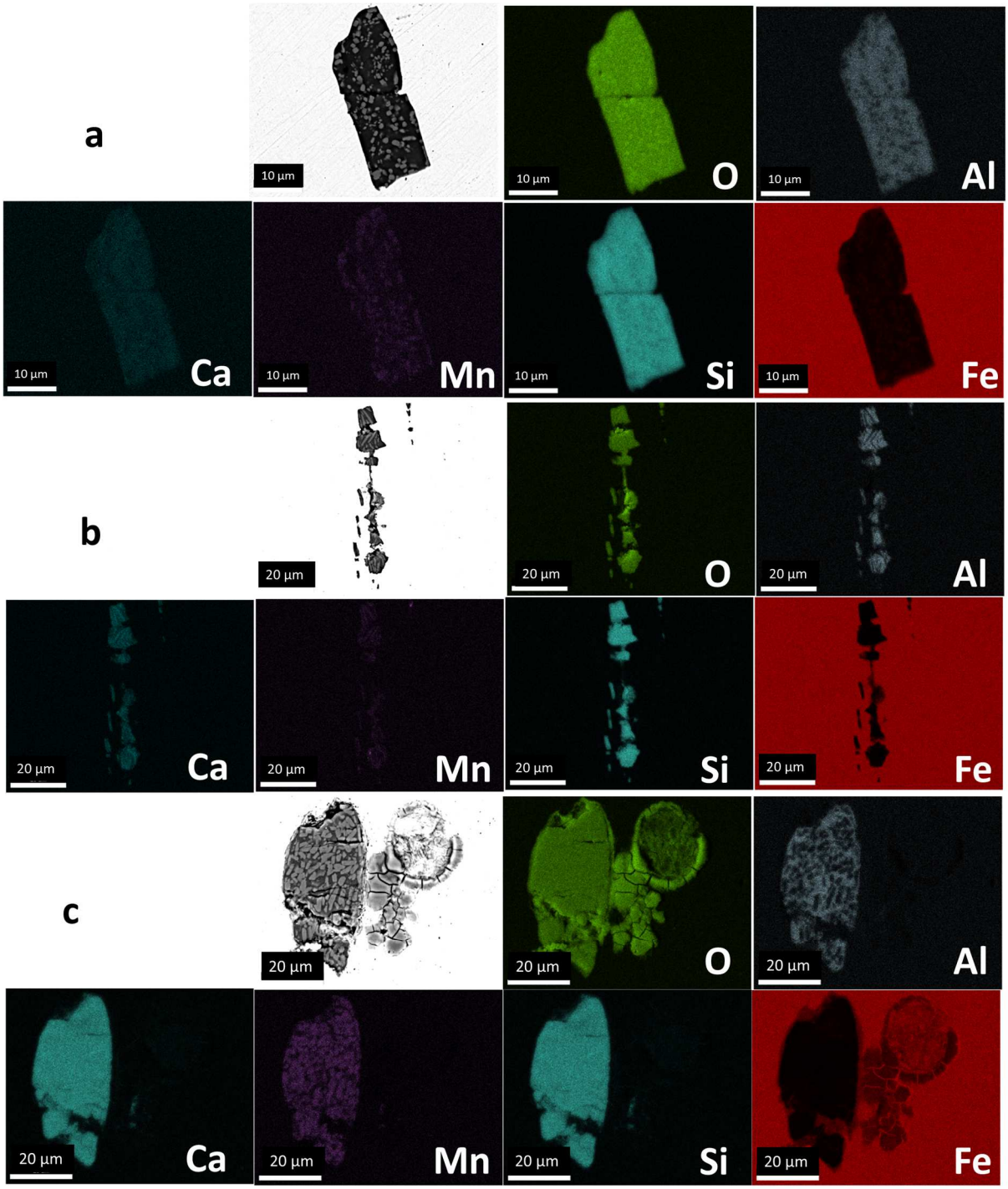

Figure 8. Detailed SEM analyses of non-metallic inclusions: (**a**)—BSE and EDS EO micrographs of non-metallic inclusion with high Si content (sample C3, artefact c); (**b**)—BSE and EDS EO micrographs of non-metallic inclusions distribution and orientation after deformation (sample B3, artefact b); (**c**)—BSE and EDS EO micrographs showing a clear difference between non-metallic inclusions and hammerscale (sample A3, artefact a).

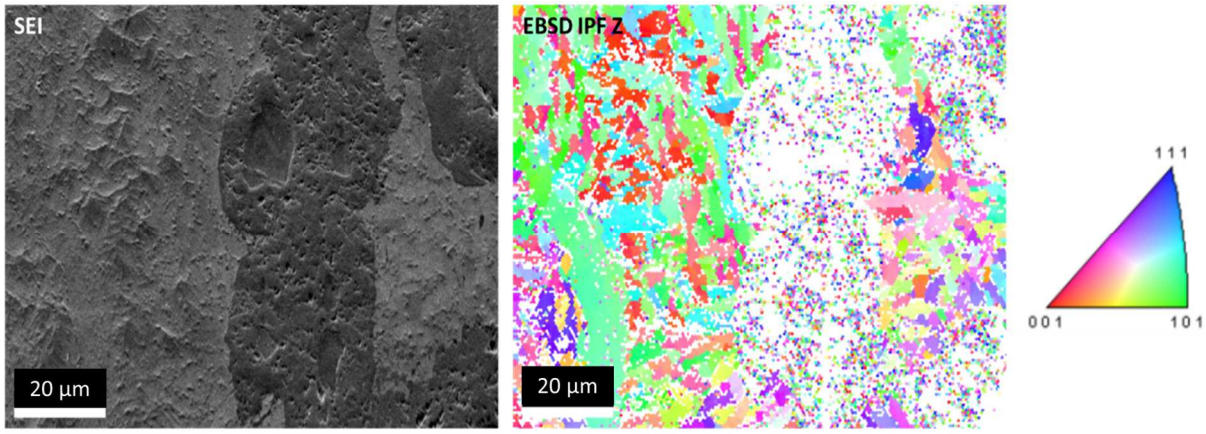

Figure 9. SEM SEI and EBSD micrographs showing the trapped scale and crystal grain orientation following the flow of deformation produced during the forging (sample A3, artefact a).

3.5. Hardness

The hardness values of the samples are shown in Table 3. The average value of five measurements on two samples taken from artefact b is 221 ± 5 HV. A slightly higher average value (236 ± 5 HV) was measured on two samples from artefact c. Less uniform measurements were observed in the three samples from artefact a. The highest hardness, 283 ± 7 HV, was measured in sample A2, followed by 262 ± 6 HV in sample A3. A considerably lower hardness (217 ± 5 HV) was measured on sample A1. This is in accordance with its microstructure, where a lower percentage of C (0.3 ± 0.05 wt.%) was determined. An even lower average hardness was measured on two samples taken from artefact d. In comparison to the other three artefacts, artefact d, with a hardness of only 185 ± 3 HV, was probably used for some other, most likely non-military, application. The hardness of preindustrial wrought iron artefacts, containing mostly ferrite, is lower than 100 HV [40].

Table 3. Micro-hardness values of investigated samples by Vickers method.

Object	Sample	Hardness [HV 0.1]
Artefact a	A1	217 ± 5
	A2	283 ± 7
	A3	262 ± 6
Artefact b	B2 and B3	221 ± 5
Artefact c	C2 and C3	236 ± 5
Artefact d	D2 and D3	185 ± 3

3.6. X-ray Radiography

X-ray investigation of the artefacts revealed further evidence of extensive corrosion damage, delamination, and internal cracks in artefacts a and b (Figure 10a,b), reinforcing previous observations made during visual inspection. Figure 10c shows the X-ray image of artefact c, whose original purpose cannot be identified more closely due to its fragmentary nature. It also provided final proof that artefact d (Figure 10d) is indeed part of a lock, as the internal mechanism is clearly visible on the radiographs.

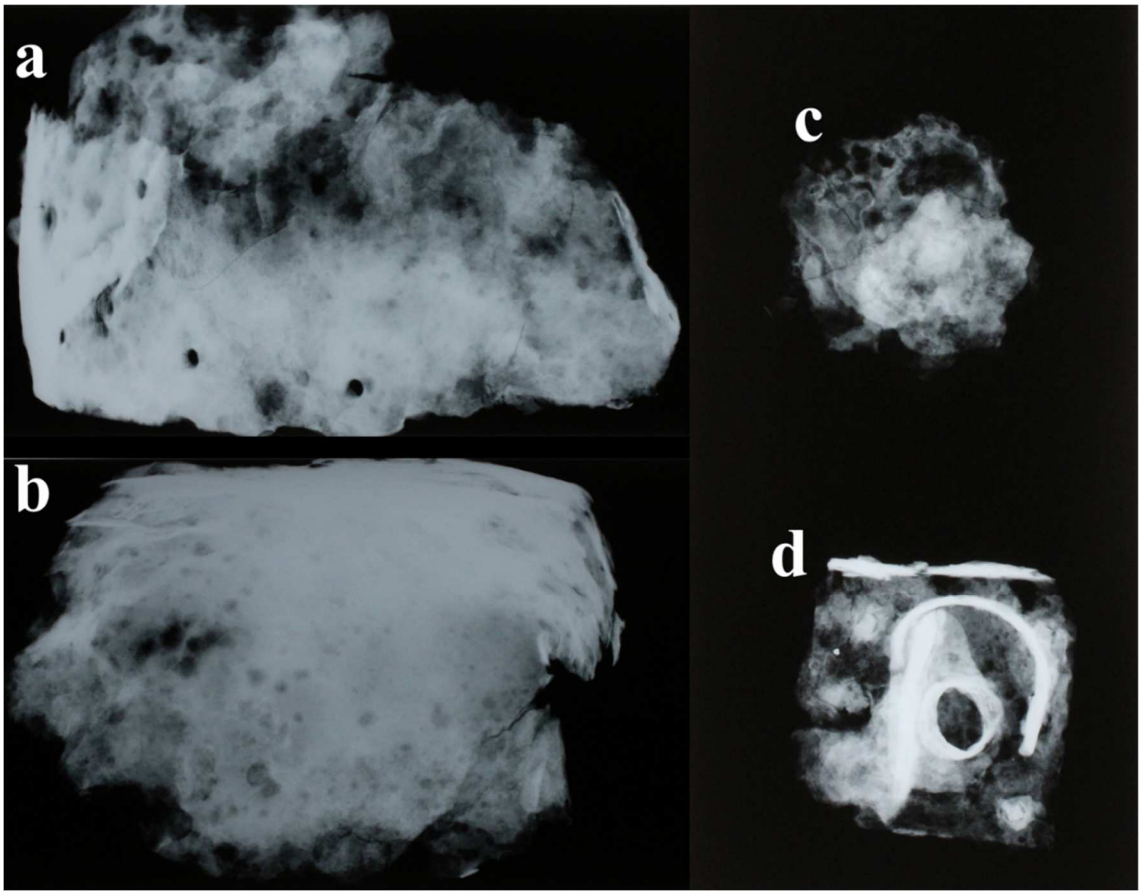

Figure 10. Radiographic photos: (**a**)—extensive corrosion damage (artefact a); (**b**)—delamination and internal cracks (artefact b); (**c**)—nondescript iron fragment (artefact c); (**d**)—internal mechanism of lock (artefact d) (Radiography: Janko Vodišek (IMK), photo: Eva Menart).

4. Discussion

Technically, all artefacts consisted of heavily corroded steel sheets, with some exhibiting multiple severely delaminated layers. Due to their circular shapes, some fragments (Figure 2a,b) were initially suspected to be parts of a helmet [41–43]. However, this assumption was dropped after closer examination, as the fragments were made of different, thicker stock. The shape was also considerably distorted due to damage and/or post-burial conditions and did not seem to fit the proportions of a human cranium. Some artefacts, such as object c from Figure 2, are a small fragment that could have belonged to one of the other items in the group or even some other artefact entirely. The lock (Figure 2, object d) was the only find in the group whose purpose could be determined more precisely. All four artefacts consisted of heavily corroded steel sheets, which made thickness measurements much more difficult than is normally the case with better-preserved or professionally restored museum objects [41]. Nevertheless, the overall impression is that all the analysed objects were originally made from quite thin stock. However, in some areas, this was joined into multiple layers, which indicates that the sheet was folded several times to increase its thickness.

However, more advanced analytical techniques may reveal important clues to the material composition and manufacturing methods of archaeological finds. For instance, the hardening effect of alloying elements in the chemical composition of steels [44] and cast iron from steel cementation furnaces have been researched to some extent by using EDS [45]. Even deeper insight into the mechanical and thermal processes involved in the manufacture of historical artefacts might be inferred from EBSD analyses, specifically in

investigating the crystal orientation and forming processes, which as yet represents an entirely novel and promising approach.

The present study underlines the importance, as well as the various limitations, of metallurgical analysis as a means of interpreting archaeological finds. The results of the analysis provide many important clues as to what the investigated fragments were originally intended for and what types of artefacts they belonged to. Nevertheless, they cannot answer these questions conclusively by themselves. To do so, they need to be evaluated in a wider historical context and our knowledge of the late medieval and early modern material culture.

The thick layer of corrosion products often makes the interpretation of excavated iron artefacts a difficult task. The finds from Kozlov Rob are a stark reminder of this problem, particularly as the iron artefacts from this site are generally poorly preserved due to unfavourable soil conditions. In several cases, this has also hampered the preparation of metallographic samples. Every effort was made to remove samples from sections with a well-preserved metal core, confirmed initially with a magnet. However, due to the magnetic properties of Fe_3O_4, this method is not always successful in differentiating between intact iron core and corrosion products.

The XRD analysis shows peaks of magnetite and hematite for all samples. Due to the high iron content, we can assume that they are Fe_2O_3 and Fe_3O_4, both stable between 1600 °C and room temperature. These corrosion products are often present on archaeological iron finds. Additionally, wüstite peaks (FeO stable from 1400 °C to 570 °C) [46], are observed in artefact b, and d. FeO forms at elevated temperatures and may be identified as hammerscale, likely produced during the forging process [39]. A cohenite peak (metallography and EDS analysis confirmed cementite—Fe_3C) is visible in the spectra of artefact c. Cohenite (Cementite, Fe_3C, iron carbide), commonly found in Fe-C alloys, is integral to the steel microstructure. The body-centred cubic (BCC) peaks were observed in all four spectra. Further chemical and microstructural analysis revealed that it was ferrite (α-Fe). This is a good indication that we are dealing with low-carbon steel without the addition of alloying elements typical of modern steels.

SEM EDS analysis also confirmed the presence of other oxide phases in the form of non-metallic inclusions in the iron matrix. These consist of elements that may have originated from iron ore, clay, ash, and flux agents, such as lime, they were introduced during the iron smelting process [17,47]. These oxides are based on Al, Mn, Si, Fe and Ca. They are a small part of the artefacts and cannot be detected by XRD.

It seems plausible that artefact a indeed belonged to a helmet of some kind, most likely a rather simple 'pot' or cabasset worn by arquebusiers and other lightly armed troops during the late 16th and 17th centuries [42,48]. This hypothesis is confirmed first by the shape of the fragment, corresponding well to the lower section of such a helmet, complete with several holes required either to attach the padded lining or a separate metal brim joined to the iron skull with rivets. Secondly, the artefact is made from a relatively high-quality, even if quite heterogeneous, material corresponding to medium to high-carbon steel. The high carbon content of the steel is evident from Figure 6c, and the metallographically estimated C content is given in Table 1. The microstructure consists of pearlite (eutectoid consisting of α-Fe and Fe_3C) and ferrite (α-Fe), which means the metal was not quenched to achieve higher hardness. Nonetheless, it has Vickers hardness from 217 to 283 HV, harder than ordinary wrought iron that typically achieves highest values of 180 HV [19]. The hardness of the lower carbon parts A1 (around 0.3%C) indicates some degree of strain hardening [49]. For example, high-end 16th century heat-treated armour with similar carbon contents reached hardness above 500 HV [19,29,36]. This would have been a fairly typical material for the production of body armour and head defences during the late Middle Ages and the early Modern Period, certainly superior to plain wrought iron generally used in the manufacture of inexpensive 'munitions-grade' armour [19,50]. To give a view of how iron objects can be hardened, an example, a 17th century Japanese sword has 154 HV in the low carbon regions and 285 HV in the high carbon region with a "slow cooled"

(ferritic and pearlitic microstructure) areas. Meanwhile, the "faster cooled" (troostite, now known as fine pearlite) high carbon areas have 310 HV, while quenched (martensitic) tip has a hardness of 724 HV [51]. Cold working (hammering at room temperature) will also increase the hardness of steel (hardness can rise to over 250 HV), but it will severely reduce ductility and cause the object to break instead of buckle during use. Cold working offers the advantage of making thin walls, but to ensure better ductility of the thin-walled iron objects, they must be annealed so the microstructure recrystallises (540 °C for low carbon steel) [52].

Artefact b was made from much thicker stock. In all likelihood, it would have been too heavy for a practical head defence, and its shape seems somewhat unsuitable for that purpose, even if taking into account the mechanical damage and distortion. Nevertheless, it was made from relatively high-quality steel with a fairly high C content that would have been quite suitable for the manufacture of armour or a tool subjected to heavy use, as opposed to other non-military or less demanding applications such as a metal bucket or cauldron. The microstructure revealed a predominantly pearlitic microstructure with a relatively high hardness of 221 HV, which indicates a lack of cold-work strain hardening [48].

Artefact c could have belonged to either a or b, though more likely to the latter considering its thickness. Nevertheless, one cannot exclude the possibility that it was originally part of some other object entirely.

The identification of artefact d is the least problematic. It represents the remains of a simple lock, most likely installed in a wooden door. It was made from a lower-quality material than the rest of the group, no doubt due to the lower functional and structural requirements expected of the finished product.

All the analysed objects were made from medium to high carbon steels typical of the preindustrial period, excluding the possibility of later contamination of the archaeological site at Kozlov Rob. The two perforated steel plates from the same location that have been the subject of earlier research were made from very similar materials, reinforcing the hypothesis that they all date from the time of permanent military occupation of the hilltop before the second half of the 17th century [10].

It is similarly worth noting that in most cases, except for the lock fragment, the objects were made from a relatively high C grade of steel well adapted to the production of body armour and heavy-duty tools. It seems that the castle armoury at Kozlov Rob was well stocked with military equipment, and even older, obsolete, or damaged items were apparently reused for various purposes on the spot, as demonstrated by the breastplate reworked into a vent cover. Such recycling could well explain the considerable number of fragmentary objects made from relatively high-quality steel sheets uncovered at the site.

5. Conclusions

Archaeological finds from Kozlov Rob castle, originally built in the 12th century, present an interesting challenge for interdisciplinary research combining the archaeologist's perspective with the analytical tools of the metallurgist. Detailed investigation of seemingly insignificant, unrecognisable fragmentary artefacts focused on their visual appearance, microstructure, mechanical properties, and craftsmanship used in their manufacture has resulted in the following observations:

Accurate thickness measurement of heavily corroded steel sheets is very difficult in practice. As confirmed by X-ray radiography, artefact a (helmet) was made from a steel sheet composed of multiple layers. On the other hand, no such layered structure could not be observed in the case of artefact d (lock), indicating a different sort of application and workmanship.

As calculated from the microstructural constituents of the analysed steels, their C content is between 0.30 wt.% ($\pm$0.05) and 0.65 wt.% ($\pm$0.11). Accordingly, the hardness values range from 185 $\pm$ 3 HV to 283 $\pm$ 7 HV.

Cohenite, decarburised zones, and the shape of the observed ferrite in the microstructure are typical of forged products and indicate that the final products had been heat-treated at the end of the manufacturing process.

Dating of the artefacts into the medieval or early modern period is confirmed by the presence of non-metallic inclusions, mostly Si or Fe oxides. These are indicative of the smelting techniques used in the pre-industrial era to produce an iron bloom, later reworked into semi-finished and final products.

The presence of a helmet and fragment of a flintlock mechanism shows military presence on the site, which is also attested by other archaeological finds of arms and armour documented over the last several decades.

Author Contributions: Conceptualization, J.K. and T.L.; methodology, J.K., T.L. and M.M.; validation, M.M. and J.B.; formal analysis, T.L. and M.M.; investigation, J.K.; resources, T.L. and M.M.; data curation, T.L.; writing—original draft preparation, J.K., T.L. and J.B.; writing—review and editing, J.B.; visualization, J.K. and T.L.; supervision, T.L. All authors have read and agreed to the published version of the manuscript.

Funding: Part of the research work and the APC was funded by Slovenian Research Agency program P2-0050.

Institutional Review Board Statement: Not applicable.

Informed Consent Statement: Not applicable.

Data Availability Statement: Not applicable.

Acknowledgments: The authors would like to acknowledge Rok Alboje from Tolmin who recovered the artefacts from the construction site and notified the Tolmin Museum.

Conflicts of Interest: The authors declare no conflict of interest.

References

1. Rutar, S. *Zgodovina Tolminskega, to je: Zgodovinski Dogodki Sodnijskih Okrajev Tolmin, Bolec in Cerkno ž Njih Prirodoznanskim in Statističnim Opisom*, 1st ed.; Hilariska Tiskarna: Gorica, Austro-Hungarian Empire, 1882.
2. Trpin, D. Tolminski grad Kozlov rob v 16. stoletju. In *Trije Gradovi, Tisoč Zgodb*; Ferletic, A., Ed.; Tolminski Muzej: Tolmin, Slovenia, 2021; pp. 67–71.
3. Žbona-Trkman, B.; Kruh, A. Stanje raziskav gradov in dvorcev na območju historične Goriške I. Dobrovo, Kozlov rob, Rihemberk, Štanjel. In *Marušičev Zbornik*; Kolenc, P., Blažič Klemenc, A., Eds.; Goriški Muzej: Nova Gorica, Slovenia, 2010; pp. 195–217.
4. Štupar Šumi, N. Razvoj naselja Tolmin z gradom Kozlov rob. *Tolminski Zb.* **1997**, *3*, 45–58.
5. Sapač, I. Grajske stavbe v Zahodni Sloveniji. In *Brda in Zgornje Posočje 4*, 1st ed.; Viharnik: Ljubljana, Slovenia, 2011.
6. Žbona Trkman, B. Renesančne najdbe na Kozlovem robu. *Tolminski Zb.* **1997**, *3*, 45–58.
7. Žbona Trkman, B.; Bressan, F. Orožje z gradu Kozlov rob. In *Vojske, orožje in Utrdbeni Sistemi v Posočju*, 1st ed.; Kofol, K., Ed.; Tolminski Muzej: Tolmin, Slovenia, 2008; pp. 49–60.
8. Mlinar, M. Grajski odpad, arheologom zaklad: Izkopavanja na Kozlovem robu leta 2020. In *Trije Gradovi, Tisoč Zgodb*; Ferletic, A., Ed.; Tolminski Muzej: Tolmin, Slovenia, 2021; pp. 31–47.
9. Williams, A. Metalurške značilnosti poznosrednjeveških oklepov iz srednje Evrope. In *Vitez, Dama in Zmaj: Dediščina Srednjeveških Bojevnikov na Slovenskem*; Lazar, T., Nabergoj, T., Jerin, B., Eds.; Narodni Muzej Slovenije: Ljubljana, Slovenia, 2011; pp. 233–247.
10. Lazar, T.; Mrvar, P.; Lamut, M.; Fajfar, P. Armour plates from Kozlov rob–analyses of two unusual finds. *Mater. Tehnol.* **2016**, *5*, 767–773. [CrossRef]
11. Guštin, M. Grad na Kozlovem robu nad Tolminom, Arheološko-sanacijska dela in programi. *Tolminski Zb.* **1997**, *3*, 35–40.
12. Kramberger, D. Kozlov rob nad Tolminom. In *Gradovi, Utrdbe in Mestna Obzidja, Vodnik po Spomenikih, Dnevi Evropske Kulturne Dediščine*; Zavod za Varstvo Kulturne dediščine Slovenije: Ljubljana, Slovenia, 2008; pp. 175–182.
13. Mlinar, M.; Klasinc, R.; Štajdohar, J.; Pečar, D.; Hrženjak, T. *Prvo Strokovno Poročilo o Arheoloških Izkopavanjih na Prostoru Severnega Medzidja na Kozlovem Robu nad Tolminom (20-0267 Tolmin Kozlov rob)*, 1st ed.; Tolminski Muzej: Tolmin, Slovenia, 2020.
14. Ferletic, A. Konserviranje in restavriranje kovinskih in koščenih arheoloških najdb z gradu Kozlov rob. In *Trije Gradovi, Tisoč Zgodb*; Ferletic, A., Ed.; Tolminski Muzej: Tolmin, Slovenia, 2021; pp. 55–59.
15. Scott, D.A. *Metallography and Microstructure of Ancient and Historic Metals*, 1st ed.; Getty Conservation Institute in Association with Archetype Books: Marina del Rey, CA, USA, 1991; pp. 63–78.
16. Starley, D. Determining the technological origins of iron and steel. *J. Archaeol. Sci.* **1999**, *26*, 1127–1133. [CrossRef]
17. Roberts, B.W.; Thornton, C. *Archaeometallurgy in Global Perspective: Methods and Syntheses*, 1st ed.; Springer: New York, NY, USA, 2014.

18. Tweddle, D. The Anglian helmet form 16–22 Coppergate. In *The Archaeology of York: The Small Finds*, 1st ed.; Council for British Archaeology: London, UK, 1992.
19. Williams, A. The Knight and the Blast Furnace: A History of the Metallurgy of Armour in the Middle Ages & the Early Modern Period. In *History of Warfare*, 1st ed.; Brill: Leiden, The Netherlands, 2003. [CrossRef]
20. Checksfield, N.; Edge, D.; Williams, A. Examinations and assessment of the Wenceslaus mail hauberk. *Acta Mil. Mediaev.* **2015**, *8*, 229–242.
21. Jouttijärvi, A. Technische Untersuchung der kaiserzeitlichen Ringbrünne von Brokær. *Acta Archaeol.* **1995**, *66*, 102–105.
22. Pleiner, R. Mail of St. Wenceslaus–Metallography of Rings. *Acta Mil. Mediaev.* **2012**, *8*, 221–228.
23. Vella, D.; Degrigny, C.; Grech, M.; Williams, A. Metallurgy of armour exhibited at the palace armoury Valleta, Malta. In *Metal 04. Proceedings of the International Conference on Metals Conservation*; National Museum of Australia: Canberra, Australia, 2004; pp. 215–233.
24. Williams, A. The steel of the Negroli. *Metrop. Mus. J.* **1999**, *34*, 101–124. [CrossRef]
25. Williams, A. Further metallographic studies on early armour from Churburg. In *The Archaeology of Iron. Recent Developments in Archaeological and Scientific Research*; The Institute of Archaeology of the ASCR: Praha, Czech Republic, 2011; Volume 163–172, pp. 306–307.
26. McDonnell, G. Iron and its alloys in the fifth to eleventh centuries AD in England. *World Archaeol.* **1989**, *20*, 373–382. [CrossRef]
27. Belcher, D.L. A metallographic Study of 18th Century Woodworking Tools from the Williamsburg Collection. Bachelor's Thesis, College of Engineering and Applied Science, Lehigh University, Bethlehem, PA, USA, 1984.
28. Goll, M. Iron Documents. Inerdisciplinary Studies on the Technology of Late Medieval European Plate Armour Production between 1350 and 1500. Ph.D. Thesis, Philosophische Fakultät, Universität Heidelberg, Heidelberg, Germany, 2013.
29. Hošek, J.; Košta, J.; Žákovský, P. *Ninth to Mid-Sixteenth Century Swords from the Czech Republic in Their European Context II*; The Czech Academy of Sciences: Prague, Czech Republic; Brno, Czech Republic, 2021.
30. Abdu, B.; Gordon, R. Iron artefacts from the land of Kush. *J. Archaeol. Sci.* **2004**, *31*, 979–998. [CrossRef]
31. Dillmann, P.; L'Héritier, M. Slag inclusion analyses for studying ferrous alloys employed in French medieval buildings. Supply of materials and diffusion of smelting processes. *J. Archaeol. Sci.* **2007**, *34*, 1810–1823.
32. Alipour, R.; Rehren, T.; Martinón-Torres, M. Chromium crucible steel was first made in Persia. *J. Archaeol. Sci.* **2021**, *127*, 105224. [CrossRef]
33. Killick, D.; Fenn, T. Archaeometallurgy: The study of preindustrial mining and metallurgy. *Annu. Rev. Anthropol.* **2012**, *41*, 559–575. [CrossRef]
34. Williams, A.R.; Maxwell-Hyslop, K.R. Ancient steel from Egypt. *J. Archaeol. Sci.* **1976**, *3*, 283–305. [CrossRef]
35. Liu, H.; Chen, J.; Mei, J.; Jia, J.; Shi, L. A view of iron and steel making technology in the Yan region during the Warring States period and the Han dynasty: Scientific study of iron objects excavated from Dongheishan site, Hebei province, China. *J. Archaeol. Sci.* **2014**, *47*, 53–63. [CrossRef]
36. Kraner, J.; Lazar, T.; Zorc, B.; Fajfar, P.; Knap, M. Archaeometallurgical characterization of a 16th century suit of armour made by Valentin Siebenbürger. *J. Cult. Herit.* **2019**, *39*, 49–56. [CrossRef]
37. Park, J.S.; Shinde, V. Technology, chronology and the role of crucible steel as inferred from iron objects of the ancient site at Junnar, India. *J. Archaeol. Sci.* **2013**, *40*, 3991–3998. [CrossRef]
38. Okamoto, H. The C-Fe (carbon-iron) system. *J. Phase Equilibria* **1992**, *13*, 543–565. [CrossRef]
39. Dungworth, D.; Wilkes, R. Understanding hammerscale: The use of high-speed film and electron microscopy. *Hist. Metall.* **2009**, *43*, 33–46.
40. Kmetič, D.; Horvat, J.; Vodopivec, F. Metallographic examinations of the Roman Republican weapons from the hoard from Grad near Šmihel. *Arh. Vest.* **2004**, *55*, 291–312.
41. Lazar, T.; Kraner, J. Thickness mapping of body armour: A comparative study of eight breastplates from the National Museum of Slovenia. *Fasciuculi Archaeol. Hist.* **2019**, *32*, 129–145. [CrossRef]
42. Blair, C. *European Armour Circa 1066 to Circa 1700*, 1st ed.; B. T. Barsford: London, UK, 1958.
43. Lazar, T. *Armour from the National Museum of Slovenia*; Narodni Muzej Slovenije: Ljubljana, Slovenija, 2022.
44. Pernicka, E. Provenance determination of archaeological metal objects. In *Archaeometallurgy in Global Perspective*, 1st ed.; Springer: New York, NY, USA, 2014; pp. 238–268.
45. Thomas, C.; Hunter, R.; Gordon, R. Internal oxidation if cast iron artefacts from 18th century steel cementation furnace. *J. Archaeol. Sci.* **2012**, *39*, 2714–2721. [CrossRef]
46. Li, Z.F.; Gao, Y.; Cao, G.M.; Liu, Z.Y. High-efficiency reduction behaviour for the oxide scale formed on hot-rolled steel in a mixed atmosphere of hydrogen and argon. *Metals* **2020**, *55*, 126–1839. [CrossRef]
47. Charlton, M.F.; Blakelock, E.; Martinón-Torres, M.; Young, T. Investigating the production provenance of iron artifacts with multivariate methods. *J. Archaeol. Sci.* **2012**, *39*, 2280–2293. [CrossRef]
48. Mann, J. Wallace Collection catalogues. In *European Arms and Armour I: Armour*, 1st ed.; The Trustees of the Wallace Collection: London, UK, 1962.
49. Karlsson, B.; Linden, G. Plastic deformation of ferrite–pearlite structures in steel. *Mater. Sci. Eng.* **1975**, *17*, 209–219. [CrossRef]
50. Edge, D.; Paddock, J.M. *Arms and Armor of the Medieval Knight*; Crescent Books: New York, NY, USA, 1988.

51. Tylecote, R.F. *A History of Metallurgy*, 2nd ed.; The Institute of Materials: London, UK, 1992.
52. Campbell, F. *Elements of Metallurgy and Engineering Alloys*; ASM International: Materials Park, OH, USA, 2008.